ADVANCED FUNCTIONAL MATERIALS
www.afm-journal.de

Materials Views
www.MaterialsViews.com

Self-Sharpening Mechanism of the Sea Urchin Tooth

*Christopher E. Killian, Rebecca A. Metzler, Yutao Gong, Tyler H. Churchill, Ian C. Olson, Vasily Trubetskoy, Matthew B. Christensen, John H. Fournelle, Francesco De Carlo, Sidney Cohen, Julia Mahamid, Andreas Scholl, Anthony Young, Andrew Doran, Fred H. Wilt, Susan N. Coppersmith, and Pupa U. P. A. Gilbert**

The sea urchin tooth is a mosaic of calcite crystals shaped precisely into plates and fibers, cemented together by a robust calcitic polycrystalline matrix. The tooth is formed continuously at one end, while it grinds and wears at the opposite end, the sharp tip. Remarkably, these teeth enable the sea urchin to scrape and bore holes into rock, yet the teeth remain sharp rather than dull with use. Here we describe the detailed structure of the tooth of the California purple sea urchin *Strongylocentrotus purpuratus*, and focus on the self-sharpening mechanism. Using high-resolution X-ray photoelectron emission spectromicroscopy (X-PEEM), scanning electron microscopy (SEM), EDX analysis, nanoindentation, and X-ray micro-tomography, we deduce that the sea urchin tooth self-sharpens by fracturing at discontinuities in the material. These are organic layers surrounding plates and fibers that behave as the "fault lines" in the tooth structure, as shown by nanoindentation. Shedding of tooth components at these discontinuities exposes the robust central part of the tooth, aptly termed "the stone", which becomes the grinding tip. The precise design and position of the plates and fibers determines the profile of the tooth tip, so as the tooth wears it maintains a tip that is continually renewed and remains sharp. This strategy may be used for the top-down or bottom-up fabrication of lamellar materials, to be used for mechanical functions at the nano- and micrometer scale.

1. Introduction

Sea urchin teeth are composed of crystalline calcite with an intricate and precisely controlled three-dimensional architecture.[1–8] Three aspects of these teeth are remarkable: i) they are made of calcite, yet can grind limestone, which is also composed mostly of calcite;[9] ii) the three structural components of the teeth—the plates, the fibers, and the polycrystalline matrix between them—have been shown to be highly co-oriented from the nanometer to the centimeter scale;[10,11] and iii) the sea urchin teeth self-sharpen with use, rather than becoming dull.[12] Here we investigate how the California purple sea urchin keeps its teeth sharp by correlating the microchemical composition with morphological and mechanical observations.

The California purple sea urchin, *Strongylocentrotus purpuratus*, inhabits the intertidal and subtidal zones on the Pacific coast of North America from Alaska to Mexico.[13,14] The sea urchins in the intertidal zone often excavate burrows into the rock to protect themselves from waves and predators.[14–17]

Dr. C. E. Killian, Dr. R. A. Metzler, Y. Gong, T. H. Churchill, I. C. Olson, V. Trubetskoy, M. B. Christensen, Prof. S. N. Coppersmith, Prof. P. U. P. A. Gilbert
(previously publishing as G. De Stasio)
Department of Physics
University of Wisconsin
Madison, Wisconsin 53706, USA
E-mail: pupa@physics.wisc.edu

Dr. C. E. Killian, Prof. F. H. Wilt
Department of Molecular and Cell Biology
University of California
Berkeley, California 94720, USA

Dr. J. H. Fournelle
Department of Geosciences
University of Wisconsin
Madison, Wisconsin 53706, USA

Dr. F. De Carlo
Advanced Photon Source
Argonne National Lab
Argonne, Illinois 60439, USA

Dr. S. Cohen
Department of Chemical Research Support
Weizmann Institute of Science
Rehovot 76100, Israel

Dr. J. Mahamid
Department of Structural Biology
Weizmann Institute of Science
Rehovot 76100, Israel

Dr. A. Scholl, Dr. A. Young, Dr. A. Doran
Advanced Light Source
Lawrence Berkeley National Lab
Berkeley, California 94720, USA

DOI: 10.1002/adfm.201001546

Their teeth are utilized to bite food as well as to scrape and bore into rock. In an adult sea urchin, five teeth are held together in a jaw-apparatus called Aristotle's lantern (see Figure S1).[18] The adaptability and utility of the Aristotle's lantern has contributed to the success of sea urchins through the course of their evolution.[19–22] In *S. purpuratus,* the teeth grow continuously at the forming end at an approximate rate of 150 μm per day.[3,23] The teeth in all sea urchins are composed of calcitic plates and fibers synthesized within syncytia of odontoblast cells in the plumula—the soft tissue connected to the forming end of the tooth.[3] As each tooth grows away from its plumula, its plates and fibers are cemented together by a polycrystalline matrix,[3] comprised of 10- to 20-nm particles of calcite[9,10] in which up to 45% of the Ca atoms are replaced by Mg.[8] The precise arrangement of these three structural elements confers the teeth their remarkable mechanical function.[8]

The complex arrangement of plates, fibers, and polycrystalline matrix in the *S. purpuratus* tooth is presented here in detail. The single-crystalline components of the sea urchin tooth— the plates and fibers—are co-oriented. The plates share one crystal orientation and the fibers share another.[10] The mineral nanophase of the polycrystalline matrix is also highly co-oriented.[10,11] The polycrystalline matrix gradually fills in the space between the plates and between the fibers, after the plates and fibers have been fully formed.[3] The Mg-rich calcite nanoparticles of the polycrystalline matrix become crystalline and co-oriented via solid-state secondary nucleation, propagating out from the previously formed plates and fibers into the amorphous precursor nanoparticles of the matrix.[10] The central part of the tooth is called the stone part and it has been shown to be harder and tougher than other parts of the tooth.[4,5,8,9,12] The stone part extends across the entire length of the tooth and is continuous with the tip of the tooth. It is comprised of Mg-rich polycrystalline matrix nanoparticles, and narrow fibers that run roughly parallel to the length of the tooth. The stone part of the tooth eventually becomes uncovered as plates and fibers are shed off around the grinding tip as the tooth wears with use.

But how exactly does the sea urchin tooth maintain its sharp tip, given the relatively hard and harsh environment in which it exists? The heart of this question is a materials design problem. Which characteristics of the tooth components are involved in the mechanism of tooth self-sharpening? We used high-resolution X-ray photoelectron emission spectromicroscopy (X-PEEM), scanning electron microscopy (SEM), energy-dispersive X-ray (EDX) analysis, electron probe micro-analysis (EPMA), X-ray micro-tomography, and nanoindentation experiments, to examine the different components in the *S. purpuratus* tooth. These analyses reveal how and where the tooth breaks and self-sharpens.

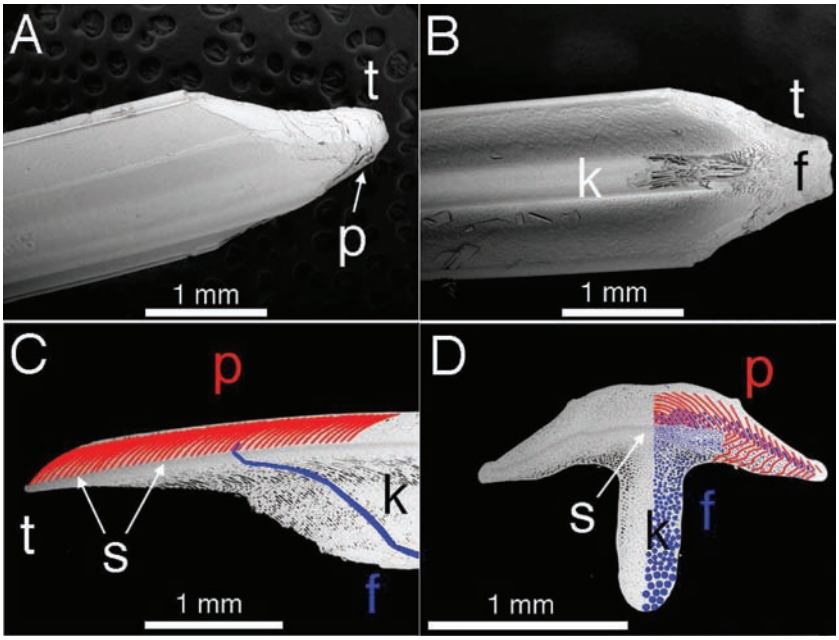

Figure 1. A,B) SEM images of the convex and concave sides, respectively, of teeth from *Strongylocentrotus purpuratus.* Labels refer to the tip (t), the plates (p), the fibers (f) in the polycrystalline matrix, and the keel (k). C,D) SEM images of the polished longitudinal- and cross-section of a tooth, showing the tip (t), the stone part (s), the plates (p), the fibers (f), and the keel (k). C and D were acquired in the back-scattered electron mode, thus they show the greater Mg concentration (darker gray level) in the stone part. In C and D several plates (red) and fibers (blue) are overdrawn on the SEM images. See also Figure S1 and S3 in Supporting Information.

2. Results

The complex arrangement of plates, fibers, and polycrystalline matrix in *Strongylocentrotus purpuratus* is laid out in **Figure 1**. Many different terms have been used to describe the various parts of sea urchin teeth. For clarity as well as consistency with the previous literature, we report these terms in the Supporting Information, and in Figure S1 and S3. Our intention is to keep the nomenclature straightforward in this report.

Each *Strongylocentrotus purpuratus* tooth is curved moderately, and has a keel that runs down the length of the concave side to lend it a T-shape cross-section.[24] The curved primary plates are present exclusively on the convex side of the tooth (Figure 1A), and they are stacked parallel to each other with calcitic fibers and a polycrystalline matrix filling the space between them. The tip of the tooth on the keel side has calcitic fibers and polycrystalline matrix, but does not have plates (Figure 1B). The fibers on this side of the tooth are curved and have a profile approximating an S-shape (Figure 1C). They extend continuously from the end of the plates to the keel.

We observe that in *S. purpuratus,* the stone part is continuous with the tip (Figure 1C), as is the case in other sea urchin species. Analyses of tooth cross-sections using energy-dispersive X-ray (EDX) analysis and backscatter electron (BSE) SEM reveal that the stone part in *S. purpuratus* is Mg-rich, as in other species, and that this Mg-rich region extends sidewise in the tooth beyond the central stone part (Figure 1D, S2, S3). Away from the tip, the plates are covered by a thick crust of polycrystalline matrix (Figure 1A)[6] that is not Mg-rich (Figure S2).

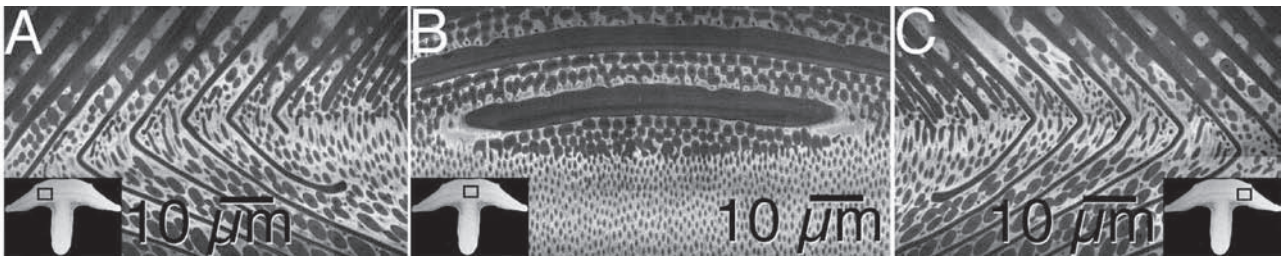

Figure 2. Magnesium maps obtained by X-PEEM. A high-Mg concentration (lighter gray level) is observed in the polycrystalline matrix surrounding the plates and fibers. A, C) Mg maps showing the areas that are 250 μm away from the center on either side, where the stone part is delimited laterally by plates that kink and extend towards the keel in a chevron shape. The black boxes in the insets indicate the position of the images in A, B, and C with respect to the whole tooth cross-section. B) Mg map at the center of the tooth cross-section, including the stone part and the first two plates delimiting it at the top.

The stoichiometry of all echinoderm biominerals is $Mg_xCa_{1-x}CO_3$, that is, Mg atoms substitute for Ca in the calcite crystal structure. Using quantitative electron probe microanalysis (EPMA) with a 1-μm electron beam size, we measured the Mg and Ca concentrations in the polycrystalline matrix of the stone part and found a value of $x = (30 \pm 3)$ mol%, whereas in the first and second plates, near the stone part, we found $x = (6 \pm 2)$ mol%. The fibers in the stone part showed $x = (12 \pm 2)$ mol%, with the Mg concentration decreasing in the prisms of the keel down to $x = (3 \pm 1)$ mol% half-way down the keel and $x = (2 \pm 1)$ mol% at the bottom of the keel. The locations of these EPMA spots are indicated in Figure S3D.

The Mg-rich stone part is bounded on the convex-side by the primary plates and on the lateral sides by the chevrons formed by the fusion of the primary and secondary plates. **Figure 2** contains Mg maps generated using X-PEEM examining a cross-section of the stone part. The dark plates and fibers reflect the relatively low Mg content of these tooth elements whereas the bright polycrystalline matrix indicates that it is high in Mg content. One can also see that the central part of the stone part is comprised of the polycrystalline matrix and small-diameter fibers. **Figure 3** is a backscatter SEM image, which, in agreement with the Mg maps in Figure 2, shows that the lateral sides of the stone part contain larger diameter fibers. It also shows that the center of the stone part contains the same density of fibers as the lateral side, but the fibers are much smaller in diameter (1 μm). In the central portion of the stone part of the tooth, which will ultimately be the grinding tip, the majority of space is occupied by the polycrystalline matrix.

To quantitatively test this aspect of the tooth we measured the averaged Ca and Mg concentrations in the stone part, using EPMA with a defocused beam of 10 μm in diameter, thus including many fibers and the matrix between them. The average Mg concentration was $x = (20 \pm 2)$ mol% in the stone part, which abruptly dropped down to $x = (17 \pm 2)$ mol% after crossing the first chevron-shaped plate that delimits the stone part.

It is clear from the profile of the longitudinal section in Figure 1C that, as the tooth scrapes and grinds, the tooth tip wears along the profile of the plates and the fibers to expose the stone part. In order to investigate what causes plate and fiber removal, we observed living sea urchins, and their motions, as shown in Figure S4.

The sea urchin mouthparts are known to have a range of motions.[2,17,19–21,25,26] In *S. purpuratus* we observed two different modes of motion, both resulting in wearing at the tooth tip. In the first mode—observed in all sea urchins and presumably used for grinding and biting—the five teeth move radially, namely, in an opening and closing motion. When the teeth close radially, the plates on the convex side of the tooth are arranged parallel to the motion and perpendicular to the compressive load applied at the tip.[4,5,21] We propose that this *radial motion* of the teeth wears away the inner, concave side of the teeth as hard objects and food are bitten. We also note that when the five teeth are closed, all the teeth tips fit tightly together (see Figure S1C, S1D, and S4) which may help keep the teeth sharp.

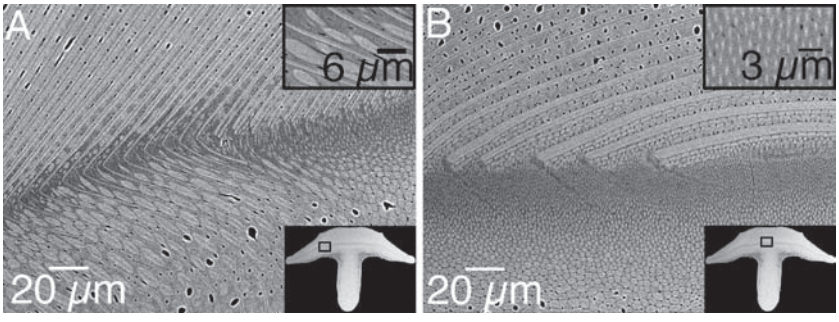

Figure 3. BSE-SEM images of the cross-section of the tooth. A) At 250 μm left of the center of the stone, where the plates start to have a chevron shape, and B) at the center of the stone part. Darker gray levels indicate areas of high-Mg concentration in the polycrystalline matrix. At the center of the stone part the fibers are much smaller, on the order of 1 μm in diameter (top inset in B), and they gradually increase in size towards the keel. Towards the left or the right, 250 μm away from the center, the Mg concentration in the matrix itself appears to be constant (B), but at this location the diameter of the fibers abruptly increases to 3 μm or more (top inset in A). The bottom insets in A and B show where the corresponding regions are located in the cross-section of the whole tooth.

A second mode of motion that plays a role in the self-sharpening of the teeth is termed here *lateral motion*. This motion is observed when Aristotle's lantern rotates, shifts, and tilts while the teeth are closed (Figure S4). This second mode of motion has been observed in sea urchins that bore into rock[17] and in other sea urchins as well.[21] This exposes the convex sides of the teeth for lateral scraping and grinding of the hard rock surface, and results in tooth abrasion.

Both radial and lateral motions may abrade the sides of the tooth tips, as they open and close into a tight fit, and as they are

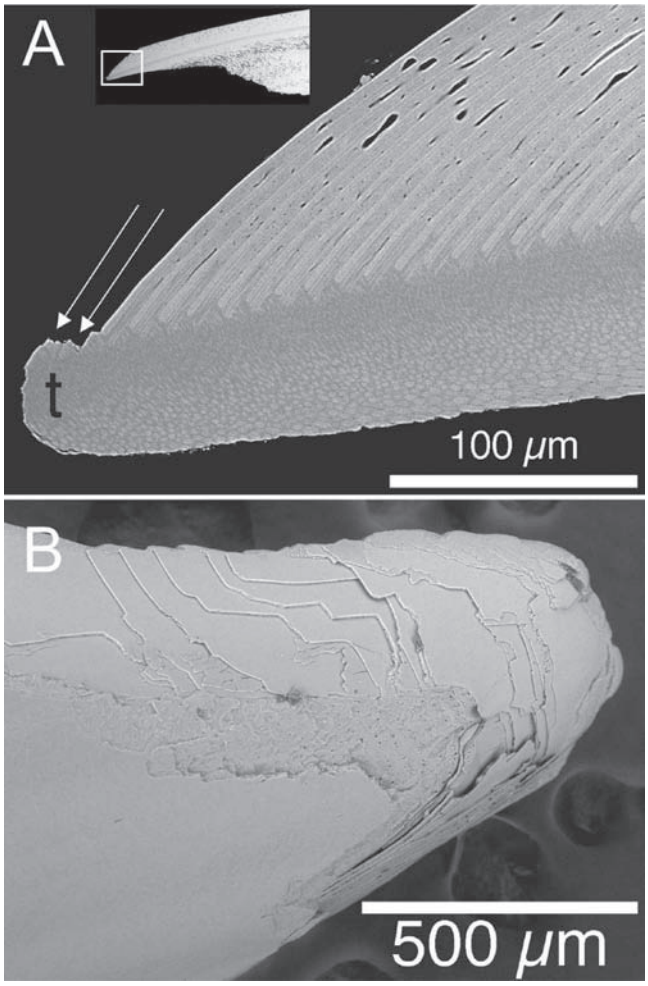

Figure 4. A) The convex side of the tooth tip, at the top in this longitudinal section, sheds one primary plate at a time. Previously shed plates have left a clear and sharp mark near their stone-part ends (arrows) and an equally sharp and smooth surface along their entire length, which defines the profile of the convex side of the tooth tip. Repeated shedding of plates, one at a time, preserves the tooth convex-side profile, thus maintaining the tooth sharpness. Furthermore, in this BSE-SEM image the Mg-rich stone part appears darker. It is evident that the grinding tip (t) is only comprised of Mg-rich polycrystalline matrix and small fibers, and no plates. Mg-rich calcite in the stone part is much harder than calcite, thus grinding is performed by the hardest part of the tooth. The white box in the inset shows the position of the imaged area in the longitudinal section of the tooth. B) The tip, seen here from the convex side, is clearly not continuously breaking but discretely, shedding plates one at a time. Plate shedding does not start at the tip. Rather, it starts behind the tip, approximately at the center of this image. It therefore cannot be provoked by the radial motion of the teeth opening and closing in the Aristotle's lantern, and must be provoked by the lateral motion of the lantern.

closed and move laterally. In both motions the sides of the tips rub against one another, resulting in the tip side tapering as observed in Figure 1A and 1B. The radial and lateral motions that result in teeth abrading against hard surfaces will fracture off pieces of the tooth near the tip. However, it is the structure of the tooth itself that determines where exactly it breaks off and renews itself, resulting in self-sharpening. **Figure 4**A displays the profile of a tooth in a longitudinal section. It is evident that the tip profile on the convex side is delimited by the smooth surface outline of a single plate. Close examination reveals that plates break away one at a time. The front (left in Figure 4A) of the plate constitutes a "weak link" in the structure. This is where the polycrystalline matrix detaches and is shed. Furthermore, from the morphology of the indentations in the matrix at the stone part, indicated by the arrows in Figure 4A, it is evident that two plates and blocks of polycrystalline matrix at the back side were removed.

Figure 4B shows that the shedding of the plates and the polycrystalline matrix between them at the convex side of the tooth does not start at the tip, as would be expected if their breaking-off was the result of compressive force at the grinding tip caused by radial motion. Rather, the fracture starts from behind the tip. We saw this occur in dozens of teeth from different *S. purpuratus* specimens; therefore we infer that the primary plates are often shed as a result of the lateral motion of the Aristotle's lantern.

Figure 5C shows in detail the location of one such fracture event that has just initiated. It is apparent that a fracture occurred at the front convex side of the plate, and that it initiated from the outer end of the plate by compressive or shear stress. The crack traveled through the plate until it reached the under-surface of the plate. The crack then propagated along the plate surface, and a portion of plate and its adjacent polycrystalline matrix were sloughed off exposing the underlying plate.

The polycrystalline matrix and the fibers on the keel side of the tip also break away at preferred locations. Figure 5F and 5I show that the fibers determine the profile of the tip at the concave side, and that they too are shed in a discrete fashion, one at a time. Figure 5L shows that the same phenomenon occurs at the keel, where the fibers are thicker. The fracture in the fiber propagates along the surface of the fiber and the fiber itself is then sloughed off. It is evident that fractures preferentially propagate along the organic layers located at the surfaces of plates and fibers.[3,8] Such organic layers were invariably observed in high-resolution backscatter SEM images, enveloping each plate and fiber, as shown in **Figure 6**. In backscatter SEM images, the organic layers appear much darker than the plates, the fibers, and the polycrystalline matrix. This observation is consistent with them being comprised of elements found in organic materials (O, N, C, H) with a lower atomic mass as compared to the metals (Ca, Mg) that are abundant in the mineralized structures (see Table S1).

In order to clarify by direct observation the fracture mechanisms in the *S. purpuratus* tooth, we carried out nanoindentation experiments. Cracks were induced and their propagation across the various structural elements of the tooth was carefully followed. We used a spherical tip with a diameter of 4 μm, and an indentation depth of either 200 nm or 400 nm. This large diameter tip and small depth were chosen to produce gentle dimples in the surface and small cracks without creating extensive local damage, so that the breaking of the tooth, where it would naturally break, could be observed. In contrast, conventional Berkovich pyramidal tips[27,28] induce local cracks through high stress at the apex and vertices of the pyramid where the tip indents. Our spherical-tip indentation was chosen in order to induce cracks where tooth discontinuities exist, namely, the natural "fault lines", and not where a pyramidal tip happens

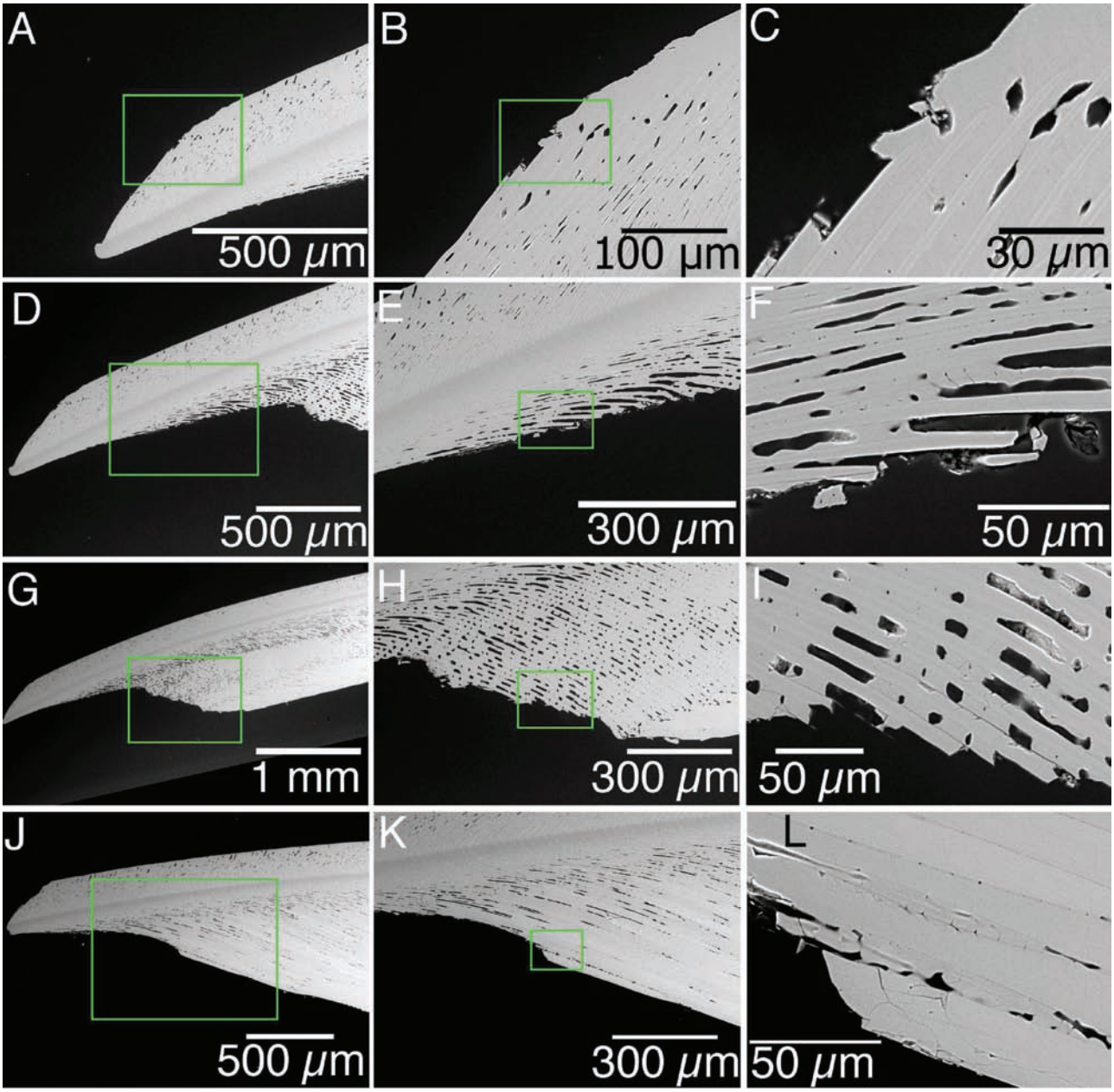

Figure 5. BSE-SEM images of longitudinal sections of *S. purpuratus* tooth tips. Each area is presented with 3 different magnifications, zoomed-out on the left and zoomed-in on the right. The green boxes indicate where the images on the immediate right were acquired. A-B-C) An area at the convex side of the tip, in which plate shedding had just begun, clearly showing that shedding starts at the outer side (top) of the plates not at the stone-part side. D-E-F) An area at the concave side of the tip showing that the fibers' profile determines where the fibers and the matrix between them discretely break. G-H-I) An area on the front side of the keel, showing the fiber-determined breaking profile. J-K-L) Another area on the front side of the keel where the fibers are thicker. Again the fracture propagates along the. surface of the fiber.

to hit the surface. The results are striking: the tip dimpled the surface, cracks propagated radially away from the dimple, and whenever a crack reached a plate or a fiber surface, the crack deflected abruptly and dramatically, often by as much as 90 degrees. **Figure 7** shows two examples of such strikingly abrupt crack deflection at the organic layers surrounding a plate and a fiber, respectively. The results of Figure 7 are representative of 43 dimple indentations, produced in three sea urchin teeth, from three different animals. Such clear and abrupt crack deflection provides strong evidence that crack deflections in *S. purpuratus* teeth occur at the surfaces of plates and fibers, where organic layers surround these calcitic components.

In addition, we consistently noticed in cross-sections of *S. purpuratus* teeth that there are conspicuous holes in the polycrystalline matrix, which were previously identified as the cell channels.[5,8] Some of these holes are apparent as dark spots

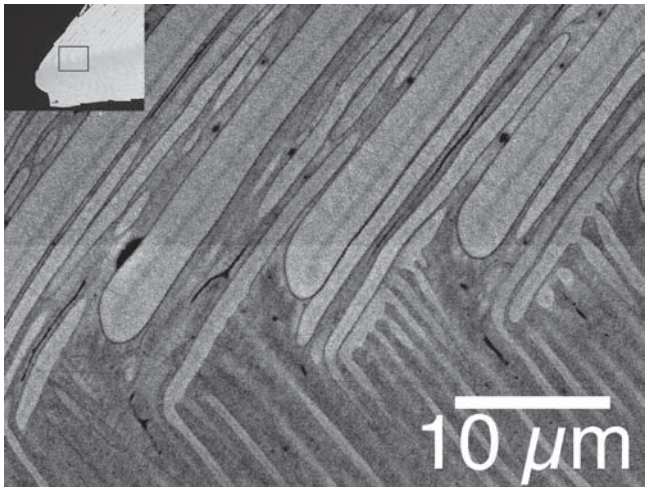

Figure 6. BSE-SEM image of the organic layers around the plates and fibers, in a tooth longitudinal section. The black box in the inset shows the position of the imaged area in the longitudinal section of the tooth. This region near the tip shows the details of plates and fibers. Notice the dark organic layers surrounding the plates, the lamellae, and the needles. These layers separate the various tooth components from the Mg-rich polycrystalline matrix that cements all components into a single rigid structure. The organic layers are darker than the Ca-rich plates and slightly darker than the matrix, consistent with the typical composition of organic molecules. In BSE-SEM images, in general, heavier elements (higher atomic mass) appear lighter in the gray level (refer to Table S1).

near the top of Figure 3A, 3B, and 4A, and near the center of Figure 4B in the polycrystalline matrix between the plates surrounding the stone part of the tooth. These holes were not observed in the stone part of the tooth cross-section (e.g., Figure 6). Because of their location, these discontinuities may very well play a role in the controlled breakaway of plates and fibers away from the stone.

To obtain a three-dimensional view of the exact location and distribution of these holes, we carried out hard-X-ray tomography on the *S. purpuratus* tooth, with a resolution of 1 μm. The X-ray micro-tomography images do not reveal contrast between the plates, fibers, and the matrix, since their densities are too similar to one another to provide X-ray absorption contrast at 20 keV. The holes, however, do stand out in these micro-tomography reconstructions. **Figure 8** shows a cross-section slice from the 3D tomography of the tooth (see Movie S1 in the Supporting Information for a fly-through movie of the 3D reconstruction, and Movie S2 for another reconstruction rotating in space). From these micro-tomography data, it is clear that holes and discontinuities of the polycrystalline matrix are abundant between the plates and in the keel, but completely absent from the stone part. This observation suggests that the holes play a role in weakening the polycrystalline matrix away from the stone part, and facilitate breaking or deflecting fractures at those locations.

3. Discussion

Wang et al.[8] pointed out that the shape of the grinding tip of the sea urchin tooth reflects the structural components (plates, fibers, and polycrystalline matrix) of the sea urchin tooth. From these observations, they theorized that the hardness of the components as well as the interfaces between the individual components would dictate the mechanism of self-sharpening. The results presented here provide experimental evidence for that theory. Our studies clearly show that the structural geometry and chemical makeup of the teeth components explain the mechanisms for maintaining sharp tips. From the data, several salient points can be concluded, as listed below.

3.1. Tooth Components Breakaway at Pre-determined Locations

Discrete shedding of plates and fibers is observed. These tooth components are pre-shaped and stacked to appropriately delimit the sharp morphology of the tooth tip, which is eventually exposed by wear. Wear and shedding also result in the exposure of the robust stone part, which becomes the tip of the grinding end.

3.2. Breakaway Locations Are Organic Layers

The break-off points are located at mechanically weak layers of organic molecules surrounding plates and fibers. These organic layers were previously described by Wang et al.,[8] Ma et al.,[9,12] and Robach et al.,[29] but their function as pre-determined breaking locations was not previously suggested. It is unclear if preferred breaking occurs within the 100-nm thickness of the

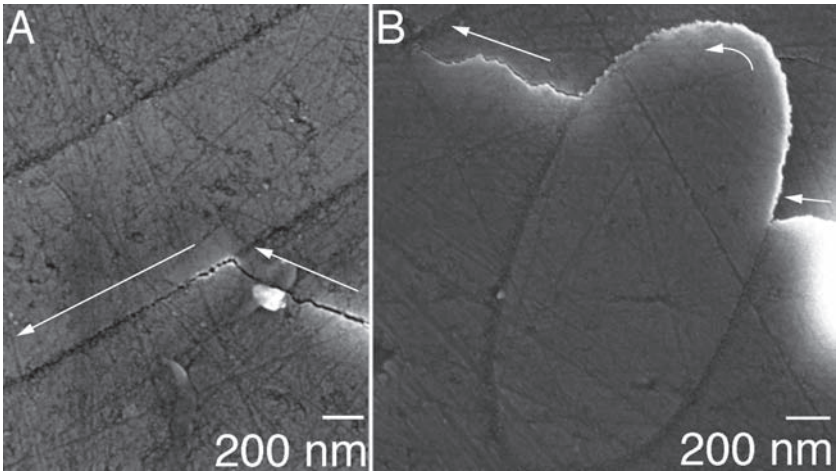

Figure 7. Secondary-electron SEM images of cracks induced by nanoindentation. In both images the crack originates from an indent in the matrix at the right hand side, and is abruptly deflected at the surface of a plate (A) and a fiber (B). The arrows indicate the direction of the crack propagation.

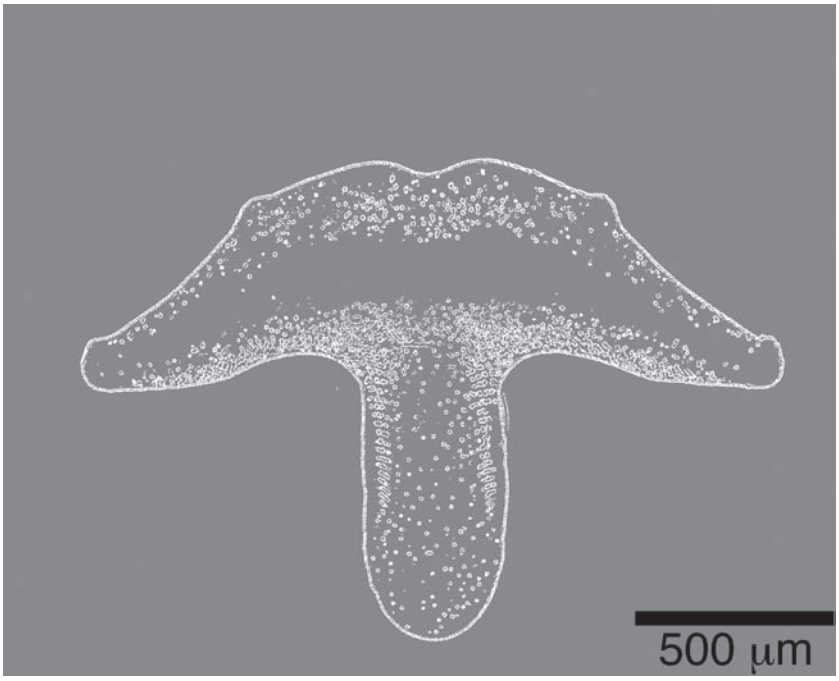

Figure 8. An *S. purpuratus* tooth cross-section extracted from the full 3D reconstruction of the tooth by micro-tomography. The white pixels indicate the locations of abrupt density variation, that is, the profile of holes in the tooth. Notice that there are no holes in the central stone part, where fracture and presumably porosity must be prevented, whereas they occur everywhere else in the tooth. See Movie S1 (Supporting Information) for an animated 3D-reconstruction, flying-through along the tooth axis, and Movie S2 for another animation with a segment of the tooth rotating in space.

organic layer, or at the outer, or inner organic-mineral interface around each plate and fiber.

3.3. Nanoindentation Shows Abrupt Crack-Deflection at the Organic Layers

Even if cracks start elsewhere, when they encounter the organic layers at the surface of a plate or a fiber, they abruptly kink in a direction propagating along the layers. The nanoindentation experiments showed this behavior clearly and unmistakably. We conclude, therefore, that the organic layers remain the "weak links in the chain" in the sea urchin tooth.

3.4. Lateral and Radial Motions Contribute to Tooth Abrasion

The lateral and radial motions of the Aristotle's lantern (Figure S4) promote the abrading of the primary plates, and fibers, respectively, thus constantly renewing the plates and fibers that delimit the convex- and concave-side profiles of the tooth. Lateral motions must promote plate shedding at the convex side, because shedding starts at the outer side of the plates, not directly at their tip (Figure 4B and 5C).

The tight-fitting of the closed teeth may also contribute significantly to sharpening of the teeth at the tip lateral sides, where they overlap and rub against one another during both motions (Figure S1 and S4). This mechanism whereby the hard parts of the tooth sharpen at weak links of the neighboring tooth is analogous to the self-sharpening seen in rodent (e.g., mice and rats) and lagomorph (e.g., rabbits and hares) incisors.[5,30,31] In these organisms, both top and bottom incisors grow continuously, and the hard enamel of the outer part of the bottom incisor cuts into the relatively softer dentin of the inner surface of the opposing top incisors, which leads to sharpening.

3.5. Chemical Composition and Structure of the Stone Part

Our qualitative results in *S. purpuratus* are in line with the observations in other sea urchins that the stone part of the tooth is high in Mg.[11] In addition, we see that a highly polycrystalline matrix density is achieved in the center of the stone part through reduced fiber diameters. The polycrystalline matrix in the stone part is the most robust part of the tooth. This may be the result of the high Mg concentration as suggested previously[5,8,9,11,32] or by the nanoscale texture of the polycrystalline matrix (10 nm in *S. purpuratus*, as measured by microdiffraction[10]), which provides resistance to flaws in other biominerals.[33] As the Mg-enrichment and nanophase texturing concur in the sea urchin tooth, we cannot deduce if one or both mechanisms are at work. It is useful, however, to track the position and density of the polycrystalline matrix by measuring the Mg content, bearing in mind that it may be either the composition (high Mg) or the size of the particles (10 nm) that confers robustness.

We observed an abrupt change in fiber diameter and Mg-enrichment of the calcite at the chevron-shaped plates, which provide discontinuities 250 μm away from the tooth center on both sides. These discontinuities coincide with break-away locations near the tip. We believe that the consistently observed 500-μm width of the tip is related to this structural discontinuity.

In other sea urchins the stone part of the tooth was equated to the Mg-rich region.[8,11] We note that in *S. purpuratus* the Mg-rich region is 1.5 mm wide (Figure 1D and S2) whereas the stone part, which becomes the tip, is only 500 μm wide (Figure 2 and 4B). "The robust center that becomes the tip", therefore, is a better definition of the "stone part". The fiber diameter and plate morphology observed at the edges of the stone part is an example of the precise control that *S. purpuratus* exerts over the materials properties of its teeth.

Micro-tomography of the *S. purpuratus* tooth reveals that the polycrystalline matrix between plates and fibers away from the stone part of the tooth has pores. Porous materials are known to be less structurally robust than continuous, space-filling materials,[34,35] thus it is interesting to notice that the porosity in the stone part of the sea urchin tooth is indeed very low.

4. Conclusions

The data presented here provide unprecedented mechanistic details on where and how the sea urchin tooth breaks, resulting in self-sharpening. The discontinuity at chemical interfaces guides crack propagation. By controlling the localization of fracture at the nanoscopic and microscopic scale, *S. purpuratus* controls the macroscopic morphology of the tooth tip, resulting in the maintenance of a robust and sharp tip.

Single-crystalline biominerals from many animals do not break as crystals—that is, along cleavage planes. They instead break like glass—exhibiting a smooth and often curved fracture figure termed conchoidal.[36] Spicules and spines from *S. purpuratus* exhibit conchoidal fracture, and this has been attributed to the presence of intracrystalline proteins.[37–39] The breakage of the sea urchin tooth at its grinding tip, however, is different. Whereas elements of the tooth, such as plates and fibers, may break conchoidally, the tooth tip does not. It breaks at the organic layers surrounding the plates and fibers. This structural organization helps deflect cracks and prevent catastrophic breakage of the tooth. This design also results in shaping and sharpening of the tooth tip in pre-determined locations, built into the structure of the plates and fibers as the tooth forms. This mechanism is akin to perforated paper, which, when subject to tensile stress, breaks at the predetermined locations of the perforations. All of the holes we observed were outside the stone part, which is where the tooth needs to be robust to perform its food-biting and rock-grinding function. It appears likely that the holes assist in pre-determining the breaking locations away from the central stone part.

Although there are differences in anatomy and component arrangement in the different species of sea urchin, the teeth of all sea urchins have plates and fibers cemented together by a polycrystalline matrix. The tooth self-sharpening mechanism described here in the tooth of *S. purpuratus* is thus likely to be shared by other sea urchins. A similar mechanism of breaking at pre-determined locations may also be used by the continuously forming and always sharply tipped radula teeth of chitons[40,41] and limpets.[42] These mollusks have evolved their teeth separately and independently,[42] as has the echinoderm studied here. To perform the same rock-grinding and self-sharpening functions, mollusks and echinoderms may very well have adopted convergent design strategies. This convergence, if confirmed by future studies, would be particularly compelling evidence that the teeth are optimized for their function, as the organisms evolved their teeth after diverging from a common ancestor. The strategy of breaking at interfaces in pre-determined locations may be useful in the design of synthetic lamellar materials, formed either by bottom-up or top-down approaches to materials fabrication.

5. Experimental Section

Detailed methods are described in the Supporting Information. Briefly, *S. purpuratus* teeth were extracted, fixed, embedded in epoxy and polished for X-PEEM, SEM, EPMA analysis, as well as nanoindentation. Teeth for SEM imaging and tomography of the entire tooth were extracted and cleaned by bleaching.

We used PEEM-3 on beamline 11.0.1 at the Berkeley-ALS for all X-PEEM experiments. SEM analysis was carried out either with a Hitachi TM1000 at the Electron Microscopy Lab at the University of California, Berkeley, or a Zeiss Leo Ultra 55 at the Weizmann Institute of Science (WIS). Nanoindentation experiments were also carried out at the WIS, using an Agilent XP Nano Indenter. Micro-tomography was done at the Argonne-APS on beamline 2-BM. EPMA and EDX-SEM were done at the University of Wisconsin-Madison, using a Cameca SX51 and a Hitachi S-3400N, respectively.

Supporting Information

Supporting Information including two movies is available from the Wiley Online Library or from the author.

Acknowledgements

We thank Lia Addadi and Steve Weiner for useful discussions and for reviewing the manuscript. We thank Martin Kunz and Nobumichi Tamura for diffraction experiments, and Jamey P. Weichert for the use of Amira software. This work was supported by the DOE award DE-FG02-07ER15899, NSF award CHE-0613972, and UW-Hamel Awards to P. Gilbert. The X-PEEM experiments were performed at the ALS, supported by the DOE under contract DE-AC02-05CH11231. Micro-tomography was done at the APS, supported by the DOE under contract DE-AC02-06CH11357.

Received: July 27, 2010
Revised: September 21, 2010
Published online: December 22, 2010

[1] K. Brear, J. D. Currey, *J. Mater. Sci.* **1976**, *11*, 1977.
[2] R. C. Brusca, G. J. Brusca, *Invertebrates, Second Edition*, Sinauer Associates, Sunderland, MA**2002**.
[3] E. Kniprath, *Calcif. Tissue Res.* **1974**, *14*, 211.
[4] K. Märkel, P. Gorny, *Z. Morph. Tiere* **1973**, *75*, 223.
[5] K. Märkel, P. Gorny, K. Abraham, *Fortschr. Zool.* **1977**, *24*, 103.
[6] K. Märkel, H. Titschack, *Z. Morph. Tiere* **1969**, *64*, 179.
[7] S. R. Stock, K. I. Ignatiev, T. Dahl, A. Veis, F. De Carlo, *J. Struct. Biol.* **2003**, *144*, 282.
[8] R. Z. Wang, L. Addadi, S. Weiner, *Phil. Trans. R. Soc. Lond. B* **1997**, *352*, 469.
[9] Y. R. Ma, S. R. Cohen, L. Addadi, S. Weiner, *Adv. Mater.* **2008**, *20*, 1555.
[10] C. E. Killian, R. A. Metzler, Y. T. Gong, I. C. Olson, J. Aizenberg, Y. Politi, L. Addadi, S. Weiner, F. H. Wilt, A. Scholl, A. Young, A. Doran, M. Kunz, N. Tamura, S. N. Coppersmith, P. U. P. A. Gilbert, *J. Am. Chem. Soc.* **2009**, *131*, 18404.
[11] Y. R. Ma, B. Aichmayer, O. Paris, P. Fratzl, A. Meibom, R. A. Metzler, Y. Politi, L. Addadi, P. U. P. A. Gilbert, S. Weiner, *Proc. Natl. Acad. Sci. USA* **2009**, *106*, 6048.
[12] Y. R. Ma, S. Weiner, L. Addadi, *Adv. Funct. Mater.* **2007**, *17*, 2693.
[13] P. Olhausen, R. Russo, *Pacific Intertidal Life*, Nature Study Guild, Rochester, NY**1981**.
[14] E. F. Ricketts, J. Cavin, J. W. Hedgpeth, D. W. Phillips, *Between Pacific Tides*, Stanford University Press, Stanford, CA**1985**.
[15] H. B. Moore, in *Physiology of Echinodermata*, (Ed: R. A. Boolootian), John Wiley and Sons, New York,**1966**.
[16] B. V. Nelson, R. R. Vance, *Marine Biol.* **1979**, *51*, 251.
[17] G. W. Otter, *Biol. Rev. Cambridge Philos. Soc.* **1932**, *7*, 89.
[18] L. H. Hyman, *The Invertebrates, IV. Echinodermata*, McGraw-Hill, New York **1955**.
[19] M. D. Candia Carnevali, F. Andrietti, in *Form and Function in Zoology* (Eds: G. Lanzavecchia, R. Valvassori), Mucchi Editore, Modena, Italy **1991**, 245.

[20] M. D. Candia Carnevali, G. Lanzavecchia, G. Melone, F. C. Celentano, in *Echinoderm Biology: Proceedings of the Sixth International Echinoderm Conference*, (Eds: R. D. Burke, P. V. Mladenov, P. Lambert, R. L. Parsley), A. A. Balkema, Rotterdam **1988**, 663.
[21] C. De Ridder, J. M. Lawrence, in *Echinoderm Nutrition*, (Eds: M. Jangoux, J. M. Lawrence), A. A. Balkema, Rotterdam **1982**, 57.
[22] P. M. Kier, *J. Paleontol.* **1970**, *48*, 1.
[23] N. D. Holland, *J. Exp. Zool.* **1965**, *158*, 275.
[24] J. W. Durham, H. B. Fell, A. G. Fischer, P. M. Kier, R. V. Melville, D. L. Pawson, C. D. Wagner, in *Treatise on Invertebrate Paleontology. Part U. Echinodermata 3*, Vol. 1, The Geological Society of America, Inc., New York **1966**, U211.
[25] R. D. Barnes, *Invertebrate Zoology, Fifth Edition*, Saunders College Publishing, Philadelphia, PA **1987**.
[26] M. D. Candia Carnevali, I. C. Wilkie, E. Lucca, F. Andrietti, G. Melone, *Zoomorphology* **1993**, *113*, 173.
[27] J. S. Field, M. V. Swain, *J. Mater. Res.* **1995**, *10*, 101.
[28] W. C. Oliver, G. M. Pharr, *J. Mater. Res.* **2004**, *19*, 3.
[29] J. S. Robach, S. R. Stock, A. Veis, *J. Struct. Biol.* **2009**, *168*, 452.
[30] T. Martin, *J. Mammal. Evol.* **1993**, *1*, 227.
[31] J. Z. Young, *The Life of Mammals: Their Anatomy and Physiology*, Clarendon Press, Oxford **1975**.
[32] R. Z. Wang, *J. Am. Ceram. Soc.* **1998**, *81*, 1037.
[33] H. Gao, B. Ji, I. L. Jäger, E. Arzt, P. Fratzl, *Proc. Natl. Acad. Sci. USA* **2003**, *100*, 5597.
[34] P. M. Mayhew, C. D. Thomas, J. G. Clement, N. Loveridge, T. J. Beck, W. Bonfield, C. J. Burgoyne, J. Reeve, *Lancet* **2005**, *366*, 129.
[35] M. A. Meyers, A. Mishra, D. J. Benson, *Prog. Mater. Sci.* **2006**, *51*, 427.
[36] K. M. Towe, *Science* **1967**, *157*, 1048.
[37] J. Aizenberg, in *Nanomechanics of Materials and Structures*, (Eds: T. J. Chuang, P. M. Anderson, M.-K. Wu, S. Hsieh), Springer, Dordrecht **2006**, 99.
[38] A. Berman, L. Addadi, A. Kvick, L. Leiserowitz, M. Nelson, S. Weiner, *Science* **1990**, *250*, 664.
[39] A. Berman, L. Addadi, S. Weiner, *Nature* **1988**, *331*, 546.
[40] H. A. Lowenstam, *Science* **1967**, *156*, 1373.
[41] P. van der Wal, J. J. Videler, P. Havinga, R. Pel, in *Origin, Evolution and Modern Aspects of Biomineralization in Plants and Animals: Proceedings of the Fifth International Symposium on Biomineralization*, (Ed: R. E. Crick), Plenum, New York, NJ **1989**.
[42] P. van der Wal, *J. Ultrastruct. Mol. Struct. Res.* **1997**, *102*, 147.